Supporting Information

Efficiency enhancement of wide bandgap lead perovskite solar cells with PTAA surface- passivated with monomolecular layer from the viewpoint of PTAA band bending

Huan Bi[1,2], Jiaqi Liu[1], Raminta Beresneviciute[3], Daiva Tavgeniene[3], Zheng Zhang[1,2], Liang Wang[1], Gaurav Kapil[1], Chao Ding[2], Shahrir Razey Sahamir[1], Yoshitaka Sanehira[1], Ajay Kumar Baranwal[1], Takeshi Kitamura[1], Dandan Wang[2], Yuyao Wei[2], Yongge Yang[2], Dong-Won Kang[4], Saulius Grigalevicius [3]*, Qing Shen[1,2]*, and Shuzi Hayase[1,2]**

[1]i-Powered Energy System Research Center (i-PERC), The University of Electro-Communications, 1-5-1 Chofugaoka, Chofu, Tokyo, 182-8585, Japan.

[2]Graduate School of Informatics and Engineering, The University of Electro-Communications, 1-5-1 Chofugaoka, Chofu, Tokyo, 182-8585, Japan.

[3]Department of Polymers Chemistry and Technology, Kaunas University of Technology, Radvilenu Plentas 19, Kaunas, LT50254, Lithuania.

[4]School of Energy Systems Engineering, Chung-Ang University, Seoul, 06974, Republic of Korea.

Corresponding Authors:

E-mail:

H. Bi: hbi.trans.sci@uec.ac.jp

S. Grigalevičius: saulius.grigalevicius@ktu.lt;

Q. Shen: shen@pc.uec.ac.jp;

S. Hayase: hayase@uec.ac.jp.

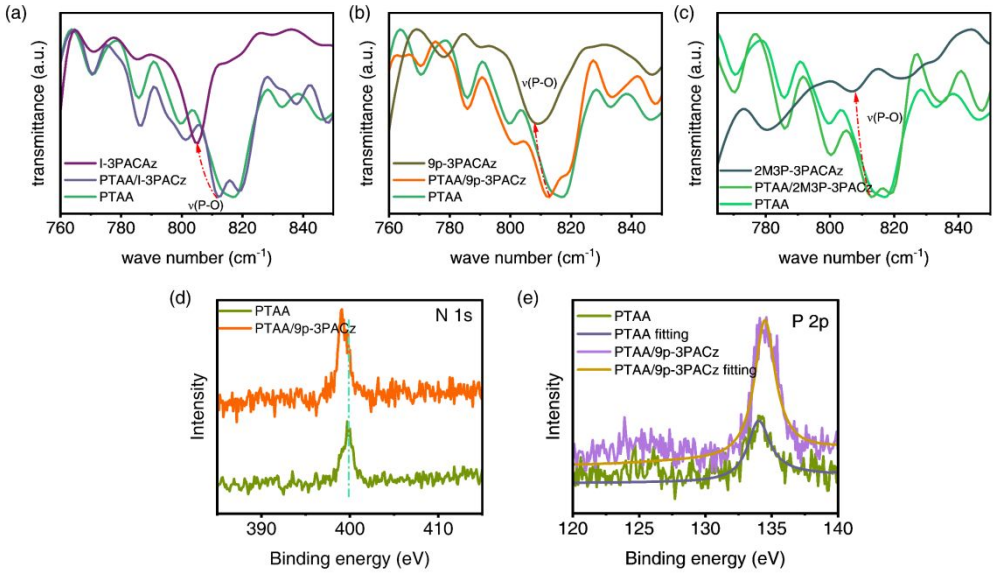

Figure S1. FTIR spectra of (a) PTAA, PTAA/I-3PACz, and I-3PACz, (b) PTAA, PTAA/9p-3PACz, and 9p-3PACz, and (c) PTAA, PTAA/2M3P-3PACz, and 2M3P-3PACz. (d) N 1s and (e) P 2p XPS spectra of PTAA film with or without 9p-3PACz modification.

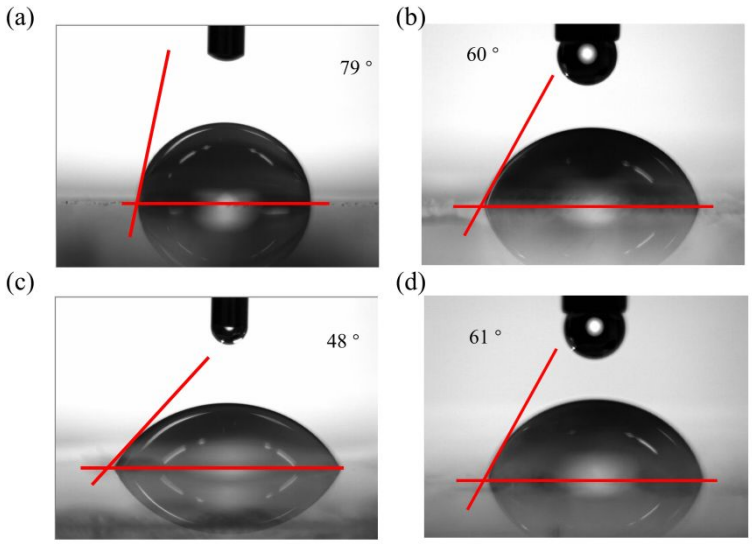

Figure S2. The perovskite solution contact angle of the substrate of (a) PTAA, (b) PTAA/I-3PACz, (c) PTAA/9p-3PACz, and (d) PTAA/2M3P-3PACz.

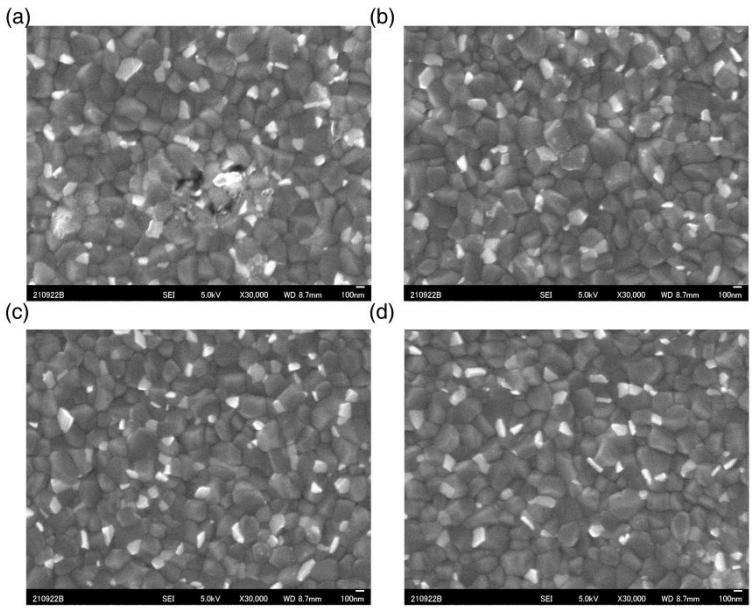

Figure S3. SEM images of the perovskite thin films deposited on (a) PTAA, (b) PTAA/I-3PACz, (c) PTAA/9p-3PACz, and (d) PTAA/2M3P-3PACz.

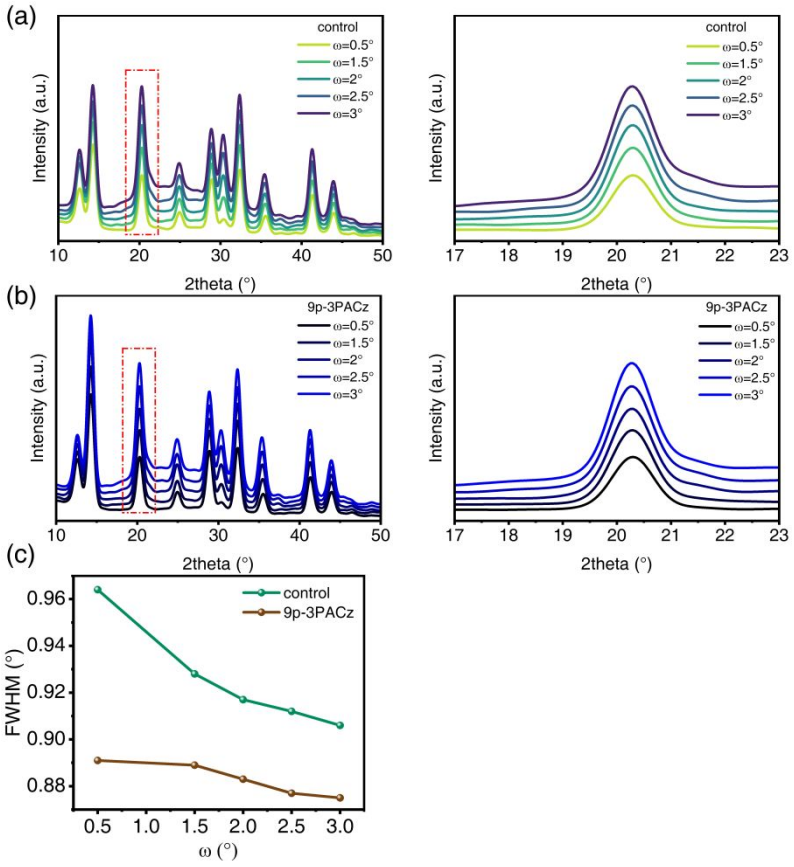

Figure S4. GIXRD patterns of perovskite films prepared on (a) PTAA and (b) PTAA/9p-3PACz. (c) The statistics of FWHM of (101).

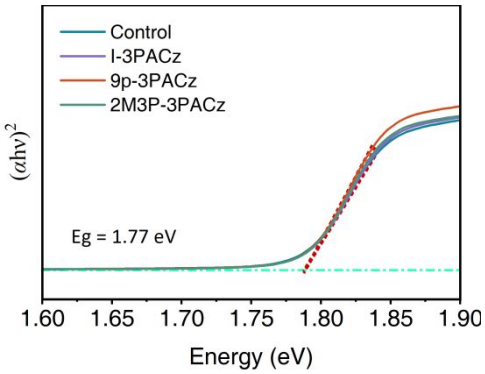

Figure S5.Tauc plot of perovskite thin film prepared on PTAA with or without surface passivation.

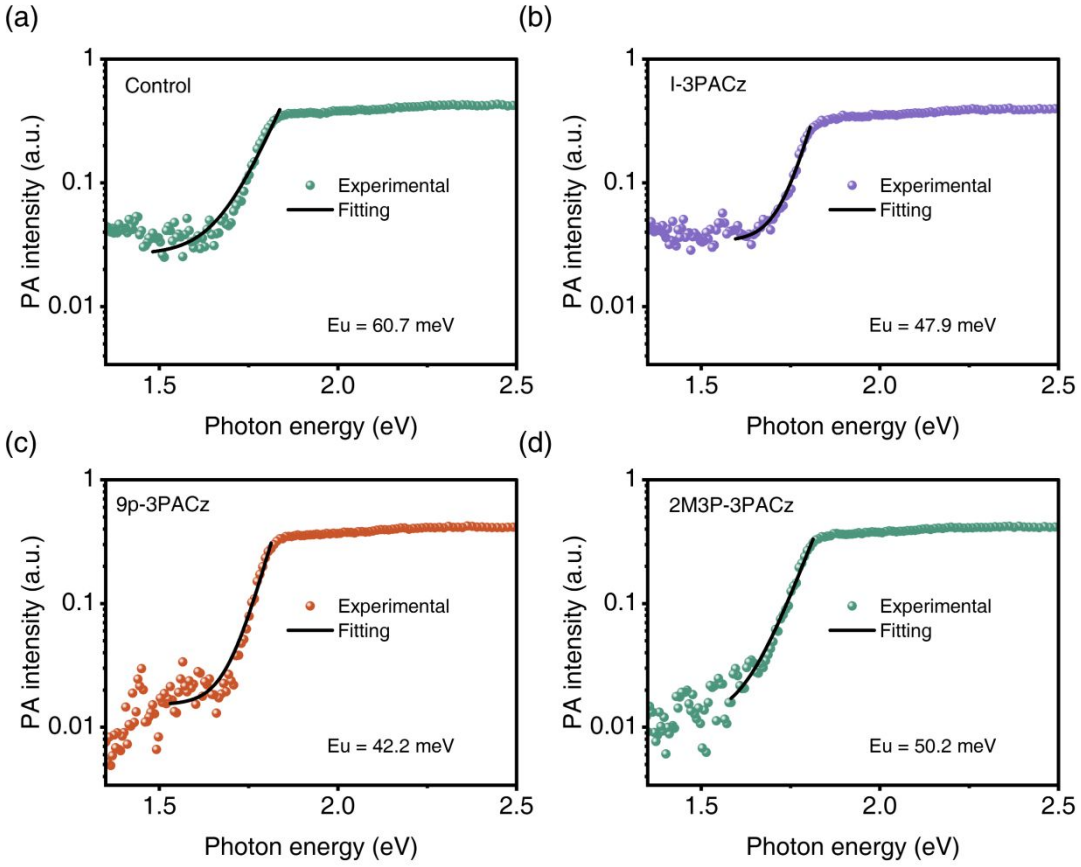

Figure S6 Urbach energy of perovskite film prepared on PTAA (a) with or (b-d) without surface passivation (b: I-3PACz; c: 9p-3PACz; d: 2M3P-3PACz) fitting from the PA data.

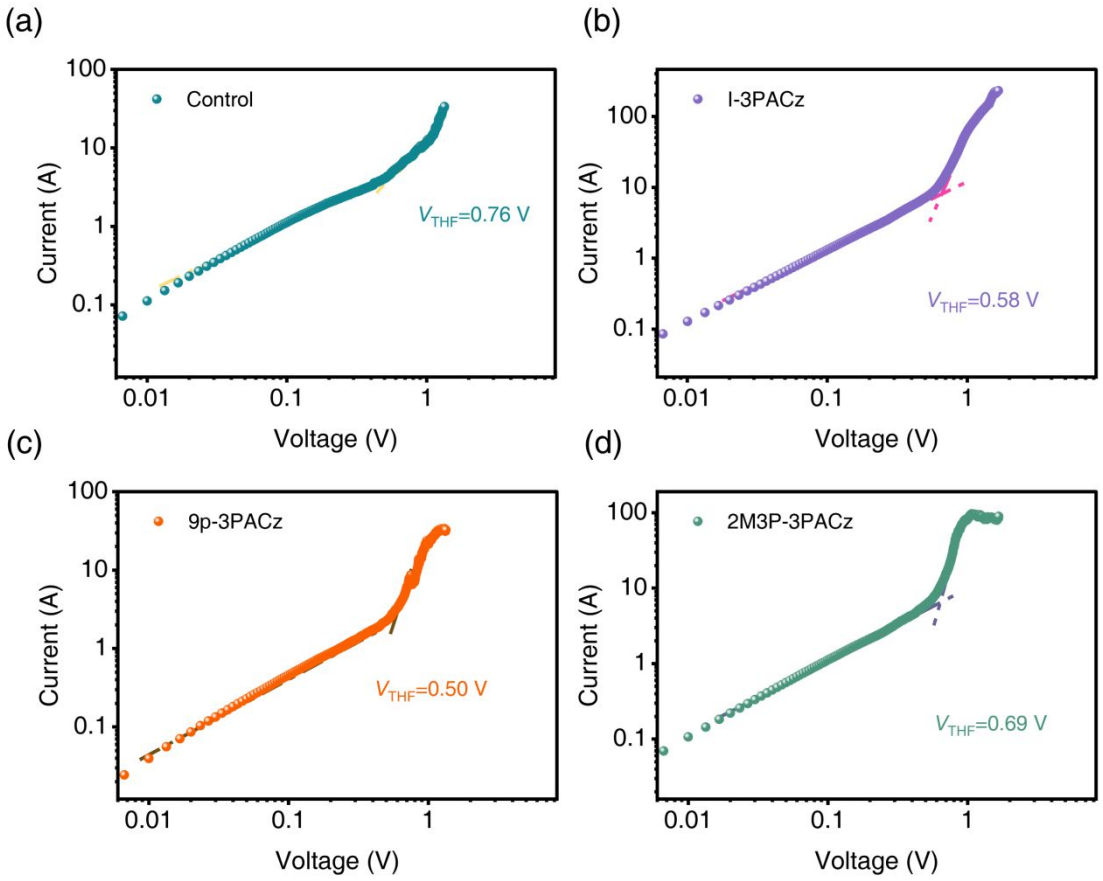

Figure S7. Dark *I-V* curves of the devices with the structure of (a) ITO/PTAA/perovskite/Spiro-OMeTAD/Ag, (b) ITO/PTAA/I-3PACz /perovskite/Spiro-OMeTAD/Ag, (c) ITO/PTAA/9p-3PACz/perovskite/Spiro-OMeTAD/Ag and (d) ITO/PTAA/2M3P-3PACz/perovskite/Spiro-OMeTAD/Ag.

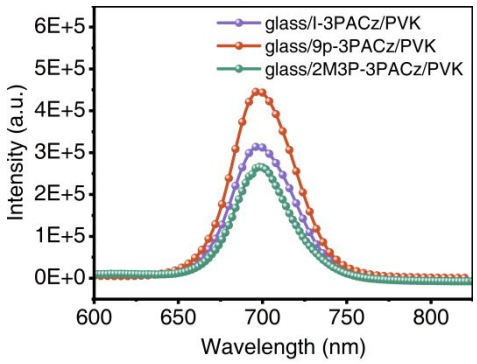

Figure S8. PL curves of perovskite film with structure of glass/monomolecular layer/PVK.

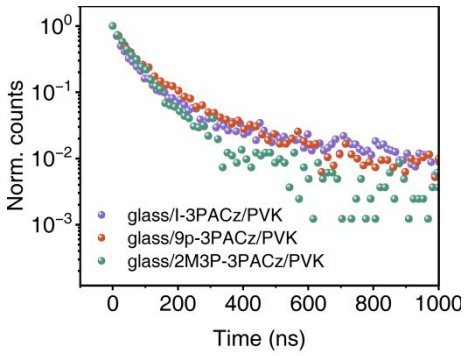

Figure S9. TRPL curves of perovskite film with the structure of glass/monomolecular layer/PVK.

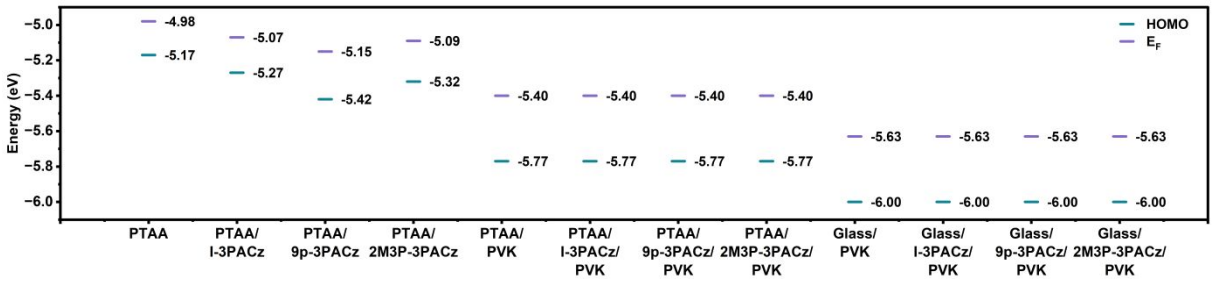

Figure S10. Homo and Fermi energy level of the PTAA and PVK with or without surface passivation. The device structure is ITO/PTAA/monomolecular layer, glass/PVK, and ITO/PTAA/monomolecular layer/PVK, where HOMO means HOMO of PVK.

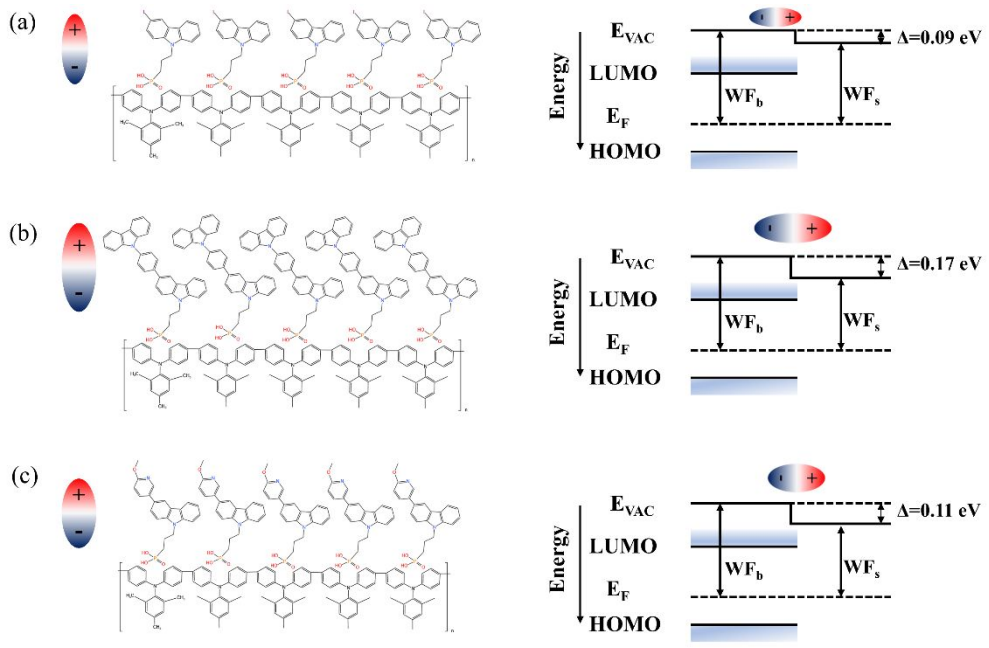

Figure S11. Effect of surface dipole on the PTAA band diagram for a) I-3PACz, b) 9p-3PACz, and c) 2M3P-3PACz. E_{VAC} is local vacuum level, Δ is vacuum level shift induced by dipolar monolayers, E_F is the Fermi level energy, HOMO and LUMO are valence and conduction band.

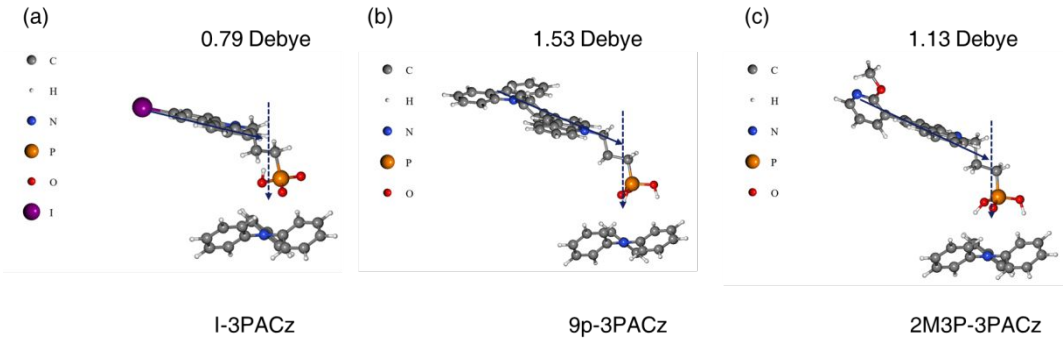

Figure S12. Dipole moment component in perpendicular direction of (a) I-3PACz, (b) 9p-3PACz, and (c) 2M3P-3PACz adsorbed on PTAA.

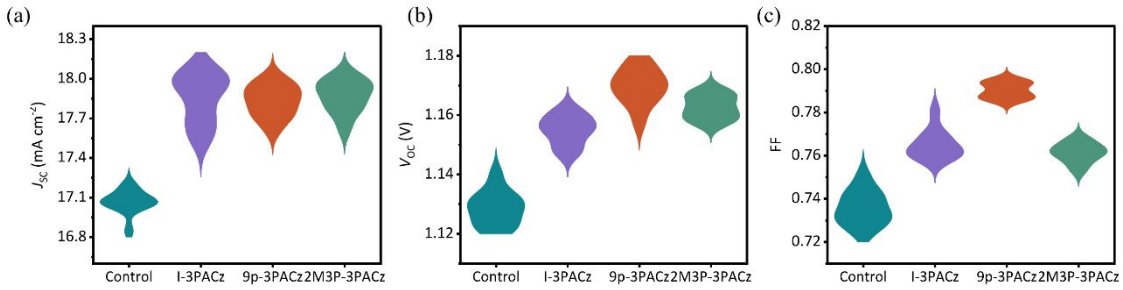

Figure S13. Statistics of (a) J_{SC}, (b) V_{OC}, and (c) FF of PSCs prepared on PTAA passivated with I-3PACz, 9p-PACz, and 2M3P-3PACz.

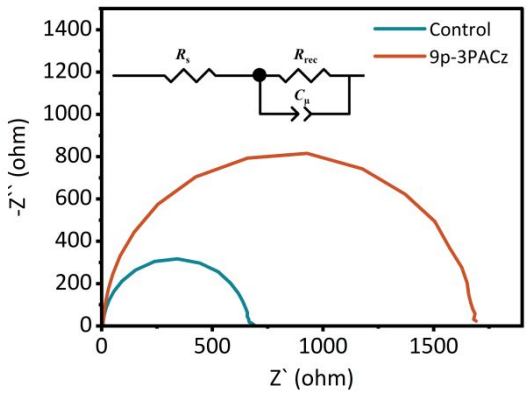

Figure S14. Nyquist plots of control device and target device measured at a bias of 0 V in the dark.

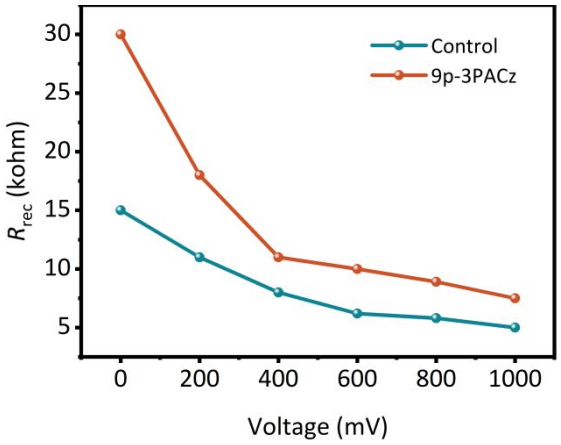

Figure S15. Recombination resistance (R_{rec}) as function of applied voltage, extracted from the Nyquist plots, fitted with the software of Fluxim.

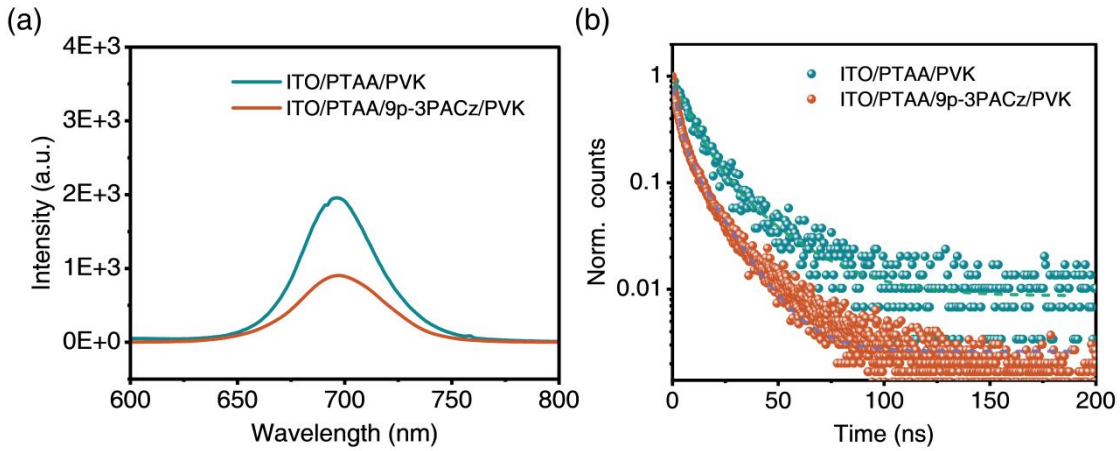

Figure S16. (a) PL and (b) TRPL spectra of perovskite films prepared on the PTAA layers without and with 9p-3PACz passivation.

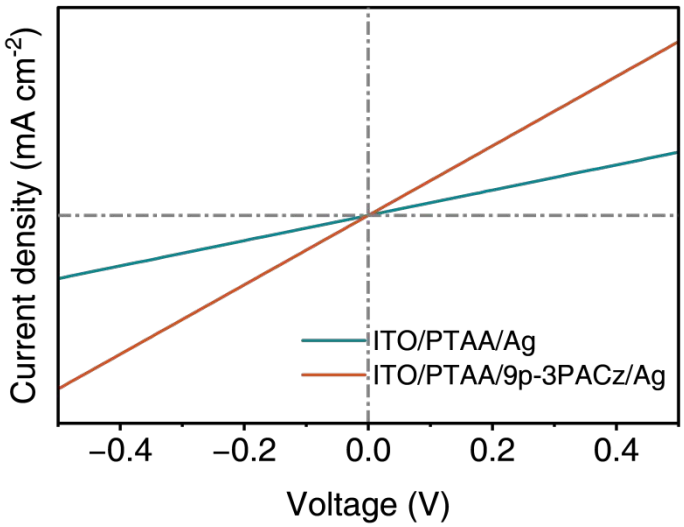

Figure S17. Conductivity of the PTAA with or without 9p-3PACz modification.

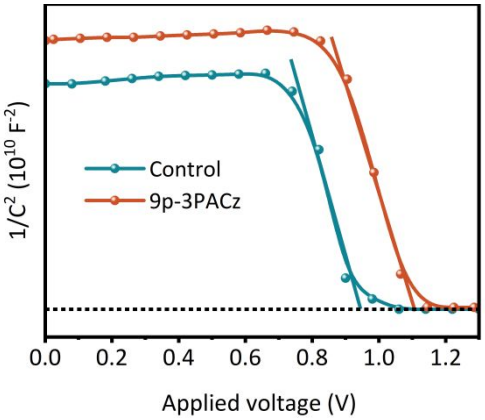

Figure S18. Mott-Schottky plots of control and target devices.

Table S1. Results fitted from TRPL spectra in Figure S8.

	Glass/2M3P-3PACz/PVK	**Glass/9p-3PACz/PVK**	**Glass/I-3PACz/PVK**
τ_1 (ns)	66.96	60.55	46.56
%	96.20	76.78	82.59
τ_2 (ns)	288.10	197.61	200.01
%	3.80	23.21	17.41
τ_{ave} (ns)	99.13	128.62	119.50

Table S2. Champion photovoltaic parameters of PSCs prepared on PTAA passivated with various molecules

	J_{SC}(mA/cm^2)	V_{OC} (V)	FF(%)	PCE (%)
Control	17.07	1.1270	75.04	14.43
I-3PACz	17.96	1.1584	76.20	15.81
9p-3PACz	17.88	1.1771	78.54	16.52
2M3P-3PACz	17.96	1.1630	75.87	15.84
2PACz	17.54	1.1425	75.52	15.13

Table S3. Results fitted from TRPL spectra in Figure S15.

	ITO/PTAA/PVK	**ITO/PTAA/9p-3PACz /PVK**
τ_1 (ns)	7.98	4.32
%	74.53	67.52
τ_2 (ns)	23.39	12.27
%	25.46	32.48
τ_{ave} (ns)	15.69	8.91

Scheme S1.

The synthesis of substituted carbazole-based SAM materials was carried out by synthetic route as shown in Scheme 1. 3-Iodo-*9H*-carbazole (**2**) was firstly obtained by a procedure of Tucker. Then, the 3-iodo-*9H*-carbazole was alkylated under basic conditions using an excess of 1,3-bromopropane to produce 9-(3-bromopropyl)-3-iodo-*9H*-carbazole (**3**). In the third step, by the means of Arbuzov reaction, the aliphatic bromide was transformed into key starting material- phosphonic acid ethyl ester (**4**). Two intermediate materials **5** and **6** were produced by Suzuki reaction of the diethyl [3-(3-iodo-*9H*-carbazol-9-yl)propyl]phosphonate (**4**) with an excess of correspondingly *9H*-carbazole-9-(4-phenyl)boronic acid pinacol ester or 2-methoxy-3-pyridinylboronic acid. The objective SAM compounds (**I-3PACz, 9p-3PACz, 2M3P-3PACz**) were prepared by hydrolysis of the esters **4-6** by using bromotrimethylsilane to obtain the phosphonic acids. The newly synthesized derivatives were identified by mass spectrometry and NMR spectroscopy. The derivatives were soluble in some organic solvents, such as tetrahydrofuran, dichloromethane, dioxane, chloroform, and methanol.